Research article

Photoluminescence research of the graphene quantum dots (GQD) interaction on the zinc oxide (ZnO) surface for application as H$_2$O$_2$ photosensor

Rolando Efraín Ramírez Garza, Sara Luisa Rodríguez de Luna, Idalia Gómez *

Universidad Autónoma de Nuevo León, Facultad de Ciencias Químicas, Lab. Mat. I, Av. Pedro de Alba s/n, San Nicolás de los Garza, 66455, Nuevo León, Mexico

A R T I C L E   I N F O

A B S T R A C T

Photoluminescence (PL) spectroscopy is one of the best methods to detect molecules due to its easiness, fast time of analysis and high sensitivity. In addition, zinc oxide (ZnO) possesses good optical properties and particularly PL emission in these materials have been exploited for their potential use as photocatalyst, light harvesting and photosensor. These PL properties enhance when graphene quantum dots (GQD) are added to ZnO. For these reasons, we investigated the PL performance of ZnO-GQD nanocomposites. In one experiment we evaluated the PL emission of solid samples ZnO and ZnO-GQD. In a second experiment, these samples were also evaluated in aqueous phase to investigate the H$_2$O$_2$ effect during an experiment lasting 170 minutes. Both experiments displayed six peaks and they were related to the same PL emission source. The PL emission peak around 415 nm was found to be principal source where GQD are interacting. By varying the GQD amount to low, medium, and high concentration, the effect of H$_2$O$_2$ acted consequently, altering the PL emission during experiment in aqueous phase. An oxygen rich environment (ORE) occurred due to H$_2$O$_2$ which oxides the ZnO surface. Low GQD concentration resulted affected by an ORE weakening the GQD-ZnO contact, decreasing PL emission. In high GQD concentration, H$_2$O$_2$ induced GQD to reach the ZnO surface, increasing the PL emission. Only medium GQD concentration prevented oxidation of ZnO and maintained the PL emission intensity constant. When H$_2$O$_2$ concentration increased, for the medium GQD concentration, an excess of charge by peroxides inhibited the charge transfer from GQD to ZnO. This inhibition produces a quenching of the PL emission.

1. Introduction

Zinc oxide is an important chemical compound since it has a myriad of applications ranging from antifungal to semiconductor-devices. These applications are accompanied by its benefits concerning the facile and green synthesis [1–3], low cost [4], low toxicity [5] and its wide band gap [6,7]. This last particularity allows the use of ZnO as photosensor by means of photoluminescence (PL) spectroscopy. The PL property of ZnO, arises principally due to oxygen vacancies as the most common source of PL emission in the visible (vis) region [8]. In the ultraviolet (UV) region emission is ascribed principally to the formation of excitons [6,9];

Available online 23 May 2024

Table 1
Sources and amount of components used for preparation of samples.

Prepared sample	Source of sample	Amount of components			Method of preparation
		Source	Water (mL)	Reagent	
HD	Graphene oxide	0.01 g	10	H_2O_2 (3 mL)	HT
D	HD	6.5 mL	NA	NH_4OH (400 μL)	HT
Dl	D	20 μL	10	NA	Water diluted
Dm	D	100 μL	10	NA	
Dh	D	500 μL	10	NA	
Z^w	Zinc acetate	50 mL of 0.125 M solution	NA	NaOH (0.5 M)	Room temp. reaction
Z^d(s)	Z^w	1 g	NA	NA	Dried at 80 °C
Z^d(l)	Z^d(s)	0.01 g	10	NA	Magnetic stirring
Z^c(s)	Z^w	1 g	NA	NA	Calcined at 500 °C
Z^c(l)	Z^c(s)	0.01 g	10	NA	Magnetic stirring

NA : not applicable

The excitation of ZnO in the UV-vis regions is a function of its application; for instance, photocatalytic application requires that semiconductors, work in the entire UV-vis spectrum, including infrared, due to most of these materials shall be exposed to sun irradiation [10]. Applications of ZnO as a light harvesting or as photoelectronic sensor normally requires only the UV region [11,12]. Consequently, ZnO presents multiple emissions and with the prospect to modify its band gap and tune PL emissions several strategies have been realized, such as the incorporation of a dopant, surface passivation or the fabrication of nanocomposites. In this sense, graphene quantum dots (GQD) have been extensively used to produce ZnO-GQD nanocomposites, because they are chemically stable and possess high electron mobility [13]. For these reasons these nanocomposites have been intensively studied in the last ten years [10,14–17]. In general, particles with sizes higher than 50 nm where mostly ZnO serves as substrate in ZnO-GQD nanocomposites, present a notable emission in the visible region and charge transfer from GQD to ZnO enhancing its conductivity [12,18–20]. There is also a generalization, that after GQD are incorporated to ZnO its band gap decreases [13,19,21]. This decrease has been ascribed to oxygen vacancies that create new energy levels below the ZnO conduction band [10]. However, a decrease in ZnO particle size might lead to an increase in the band gap and by GQD incorporation enhance the photocurrent induced facilitating its use as photocatalyst [22]. We have found that this photocurrent is not enhanced by high GQD concentration and might also be affected by the presence of a strong oxidant during a PL experiment. Similarly, it is especially important to expand such analysis by studying the role of the interaction among GQD and ZnO and its influence in PL emissions. Therefore, in this work we studied the GQD-ZnO interaction and how is affected under H_2O_2 exposure by means of PL. To achieve this task, PL studies of solids ZnO and ZnO-GQD were performed by treatment with H_2O_2 or calcination, to assign and relate emission peaks with a chemical environment in these compounds; furthermore, we extrapolated this to the same material in aqueous phase in order to explain how the system ZnO-GQD works in H_2O_2 solutions. Despite of a strong oxidant as H_2O_2, GQD were found to enhance or to conserve the PL emission of ZnO as nanocomposite through time. Specifically, GQD exert an enhancement of PL emission around 415 nm and this is done at oxygen vacancies contained in ZnO where hydrogen from GQD, is placed; moreover, we demonstrate that emissions detected at this wavelength, are the principal source of PL quenching as it was proved to detect H_2O_2. Detecting this molecule is of highly medical interest due to it is related with cellular oxidative stress, cellular ageing and cancer, among others [5,23]. We propose a mechanism of the PL enhancement and quenching from ZnO-GQD nanocomposites by studying the band gap. Finally, this study covers a possible application of photodevice to detect H_2O_2 considering the time life of the materials under this oxidant. This is crucial to evaluate if these devices perish rapidly opening a field to prepare durable or recyclable materials.

2. Materials and methods

2.1. Chemical substances

In this study the following chemical substances were used, all reagent grade and high purity: $Zn(CH_3COO)_2 \cdot 2H_2O$ (99.3%), 28 w% NH_4OH (Fermont, 98%), NaOH solid (Fermont, 98%), 30 w% H_2O_2 (Sigma Aldrich, 98%) and deionized water (Karyeth, 0.76 μS cm^{-1}).

2.2. Preparation of samples

2.2.1. Synthesis of graphene quantum dots and zinc oxide nanoparticles

Details of the preparation of solid graphene oxide are presented elsewhere [24] and from this solid, graphene quantum dots (GQD) were prepared by hydrothermal (HT) process. For the sake of clarity all samples prepared are shown in Table 1. The first step consisted of placing graphene oxide (0.01 g) inside a teflon autoclave containing 10 mL of deionized water and 3 mL of H_2O_2; this autoclave was introduced to an oven at 170 °C during 6 h. A volume of 6.5 mL of the resulting sample (named HD) was poured into a teflon autoclave and 400 μL of NH_4OH (28 w%) were added. Finally, this mixture was treated by HT process for 6 h at 170 °C. From

Table 2
Samples prepared for PL measurements.

Prepared sample	Amount of substance			Water[a] (mL)
	Zinc source	GQD source	H_2O_2 (volume concentration)	
Dh-3	NA	Dh (10 mL)		1
Z^cDl-3		Dl (10 mL)		NA
Z^cDm-3		Dm (10 mL)	1 mL (10^{-3}M)	NA
Z^cDh-3	Z^c(l) (1 mL)	Dh (10 mL)		NA
Z^c-3		NA		10
Z^cDh:0		Dh (10 mL)	NA	1
Z^c(l)		NA	NA	11
Z^d(s)[b]	Z^w (0.175 g)	NA	NA	NA
Z^c(s)[b]		NA	NA	NA
Z^d:1(s)[c]	10 mL (0.02 g	NA	10 mL (1 M)	100
Z^cD1-3(s)[c]	Z^c(s)/mL)	Dl (100 mL)	10 mL (10^{-3} M)	NA
Z^dD1:1(s)[c]	10 mL (0.02 g Z^d(s)/mL)	Dl (100 mL)	10 mL (1 M)	NA

NA : not added;

(a) Water was added to conserve a volume ratio of 1/10/1 from Zn/GQD/H_2O_2 respectively, when a substance was not added;

(b) These samples were obtained in solid phase directly (see Table 1);

(c) These samples were prepared in liquid phase and filtered to obtain the solids.

the obtained sample only the liquid phase was used, and this was named D. Volumes of 20, 100 and 500 μL were taken from D and diluted in 10 mL of deionized water to prepare the solutions Dl, Dm and Dh, respectively, in which suffixes *l*, *m* and *h* stand for low, medium and high concentrations.

Zinc oxide nanoparticles (ZnNP), were synthesized by the reaction between Zn(CH$_3$COO)$_2$·2H$_2$O and NaOH. First, 50 mL of zinc acetate solution (0.125 M) was transferred to a beaker and by gentle stirring, drops of NaOH solution (0.5 M) were added until the pH reached a value of 12. A bright white solid emerged and this suspension was stirred during 2 h. Finally, this solid was filtered and washed using 10 volumes of water with respect to the final suspension volume. One fraction of the obtained solid was named Z^w where "*w*" implies as was synthesized. A mass of 1 g of Z^w was dried at 80 °C for 20 minutes and 1 g of Z^w was calcined at 500 °C for 2 h; the obtained solids were named Z^d(s) and Z^c(s) where "*d*" and "*c*" represent a dried and a calcined sample, respectively and "*s*" stands for solid. From Z^d(s) and Z^c(s) two suspensions were prepared using 0.01 g from each solid and 10 mL of deionized water by moderate stirring for 25 minutes and these were identified as Z^d(l) and Z^c(l), respectively, where (l) is for liquid (Table 1).

2.3. Preparation of samples and photoluminescence performance

Some samples shown in section 2.2.1 were directly measured by PL spectroscopy and evaluate the H_2O_2 effect. From these samples nanocomposites were also prepared to be measured also by PL means for the same purpose. A summary of all samples prepared for PL measurements is shown in Table 2. The PL spectra were taken in a *Perkin Elmer LS55* spectrophotometer, for the solids Z^dDl:1(s), Z^d:1(s), Z^d(s), Z^c(s) and Z^cDl-3(s) in order to explore the influence of the calcination, GQD and H_2O_2 effects in the PL emission (Fig. 1). From these spectra, with the aim to determine the performance of the nanocomposites with respect to time, samples Z^c(l), Z^cDl:0, Z^cDm:0 and Z^cDh:0 were taken to evaluation at the initial point (the far left point) and this was taken as reference in Fig. 3. After this measurement, 1 mL of the H_2O_2 (10^{-3} M) solution was added to each samples and they were renamed as mentioned in Table 2 (Z^c-3, Z^cDl-3, Z^cDm-3 and Z^cDh-3); the rest of the points were measured after 20, 50, 80, 110, 140 and 170 minutes (Fig. 3); for each point of these figures the emission intensity was considered.

2.4. Characterization

The following equipment were used to characterize the materials of this work. X rays diffraction (XRD) was measured in a *Siemens D5000* equipment with a step size of 0.05° s^{-1} with a Cu X-rays source (λ = 1.5405 Å) and crystal phases were identified by the **PROFEX 5.0.2** software. Scanning electron microscopy (SEM) was taken in a *JEOL LSM 6701F*. Ultraviolet and visible (UV-Vis) spectra were taken by a *Shimadzu UV-1800* equipment. Fourier Transform Infrared spectroscopy (FTIR) was performed in a *Perkin Elmer Spectrum One* with attenuated total reflectance (ATR) complement. XPS spectra were taken with a Thermo Scientific K-Alpha instrument with a stripping capability of approximately 30 nm and Al source; the peak correction was performed using the Carbon adventitious signal (C 1s, 284.6 eV). Atomic Force Microscopy (AFM) was achieved using an AA3000 equipment. For DSC measurements a NETZSCH DSC 404F3 equipment was used with argon gas and a ramp of 10 °C/min

3. Results

3.1. Photoluminiscent (PL) emission sources from solid samples

The PL emissions were measured for solids samples treated in conditions as high H_2O_2 concentration or calcination and spectra are shown in Fig. 1. To study PL emissions, the peak at 415 nm, was taken as reference in order to detect variations on adjacent
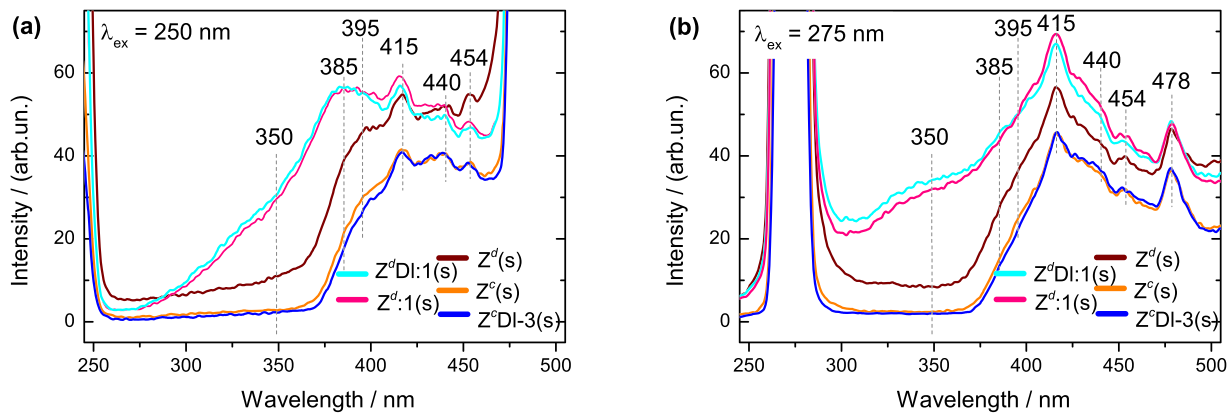
Fig. 1. PL spectra from solids samples taken as references and measured at λ_{ex} (a) 250 nm and (b) 275 nm. These spectra correspond to calcined samples Z^c(s) and Z^cDl-3(s) and to non-calcined Z^d(s), Z^d:1(s) and Z^dDl1(s). The dashed gray lines trace the emission peaks (in nm) written at the top of each line.

peaks and thus analyse the chemical environment where the emission emerges. By analysing the Fig. 1 detected peaks are designated as follow:

(A) Peak at 350 nm. This peak is related to the free and bound exciton from the near band edge emissions [9]. These emissions have been found to display a very narrow shape at very low temperatures in ZnO structures; as temperature rises a broad band emerges leading to bound exciton emission [25]. Interestingly in our case, and also found in other work [26], this emission arises due to the presence of ZnO_2. A comparison between Z^d(s) and Z^d:1(s) clearly indicates the addition of H_2O_2 implies the growth of this peak (Fig. 1a and Fig. 1b). Samples Z^d:1(s) and Z^dDl1(s), treated with high concentration of H_2O_2, were mostly converted to ZnO_2 and in Fig. S1 (see supplementary information), a representation of this process is shown in scheme 1; this is also confirmed by XRD analysis in Z^d:1(s) (Fig. 4). It is important to note that this emission peak is not presented in Z^cDl-3(s) due to the low H_2O_2 concentration used during the experiment. In spite this low concentration, H_2O_2 reacts with the ZnO surface to generate an oxygen rich environment (ORE) [27] as is proved in XPS analysis (Fig. S1 scheme 2 and Fig. 7); however, an increase in the exciton energy intensity is not observed in these solids.

(B) Peak at 385 nm. This emission is also attributed to bound exciton, which hydrogen placed near the ZnO surface, enhances the emission intensity [28]. As H_2O_2 might be dissociated into H^+ proton and $HOO^{\cdot}$ radical [29], hydrogen acceptor might be interacting with ZnO interstitials as in scheme 1 (Fig. S1). This is also inferred due to in our experiments, most of the emissions variations in the rest of the peaks detected, were attributed to ZnO and $HOO^{\cdot}$ interactions. Notwithstanding, when H_2O_2 is in higher concentration, hydrogen might enhance the emission intensity in Z^d:1(s) and Z^dDl1(s), due to it could play roles as donor, acceptor and also might be passivating nonradiative recombination centres [28,30].

(C) Peak at 395 nm. For the calcined samples Z^c(s) and Z^cDl-3(s), this peak is modified, with respect to the peak at 415 nm for Z^d(s). It is observed that for Z^d:1(s) and Z^dDl1(s) the intensity is higher than Z^d(s). In this case $HOO^{\cdot}$ radicals seem to reach intrinsics or native vacancies from the ZnO surface; this is manifested as the growth of oxygen onto the surface detected in XPS analysis (Fig. 7). The positioning of these radicals might increase the free carriers produced by electron-traps where free exciton emission emerges at this wavelength [25,31]. Although this has been found to occur at very low temperatures, in our experiment, this phenomenon was likely forced due to the use of H_2O_2 even at low concentrations. The arrival of $HOO^{\cdot}$ radicals to produce an ORE, leads to a partial depletion layer where is possible that electron-hole recombine nonradiatively which finally inhibits exciton transition. It is inferred then that this process must have a limit where high H_2O_2 concentrations produce peroxide radical leading to zinc oxidation to form ZnO_2 (Fig. 4). GQD is observed to reduce slightly the emission on both λ_{ex} (Fig. 1a and Fig. 1b) suggesting that H^+ from amine group, is interacting with ZnO vacancies. Replicas manifested as longitudinal phonon from bound exciton due to interstitial hydrogen donors, also might appear at this wavelength, however they were not present or have very low emission [25,28].

(D) Peak at 415 nm. After the calcination and the H_2O_2 exposure, a slightly higher PL emission in this peak is observed for Z^c(s) and Z^cDl-3(s) compared to Z^d(s), and of course, this is more evident for Z^d:1(s) and Z^dDl1(s) (Fig. 1b). This might be attributed to hydrogen placed onto the ZnO surface where it produces (1) a donor-acceptor pair, which is common at room temperatures [6,25,28] and/or (2) a possible surface passivation of nonradiative traps [30]. GQD slightly increase the PL emission, and contrary to peak at 395 nm, in this peak the amino group is not affected by the H_2O_2 presence. Therefore, in these sites GQD must be strongly anchored.

(E) Peak at 440 nm. This emission peak corresponds to visible blue-region where oxygen vacancies (V_O) are considered as the principal source. This has been ascribed due to V_O, are energetically more favourable to be produced from the synthesis of ZnO and therefore we assign this peak to these point defects [32,33]. These defects correspond to a neutral oxygen vacancy (V_O^x) where electron transition comes from these centres to the edge valence band [6,25,34]. For λ_{ex} = 250 nm, Z^d(s), Z^c(s), and Z^cDl-3(s), calcination, or the incorporation of H_2O_2 and GQD caused no great variations in the PL emission. This suggests that V_O are intrinsic and correspond to deep-level centres [10,21]. However, despite the low GQD concentration in Z^cDl-3(s),
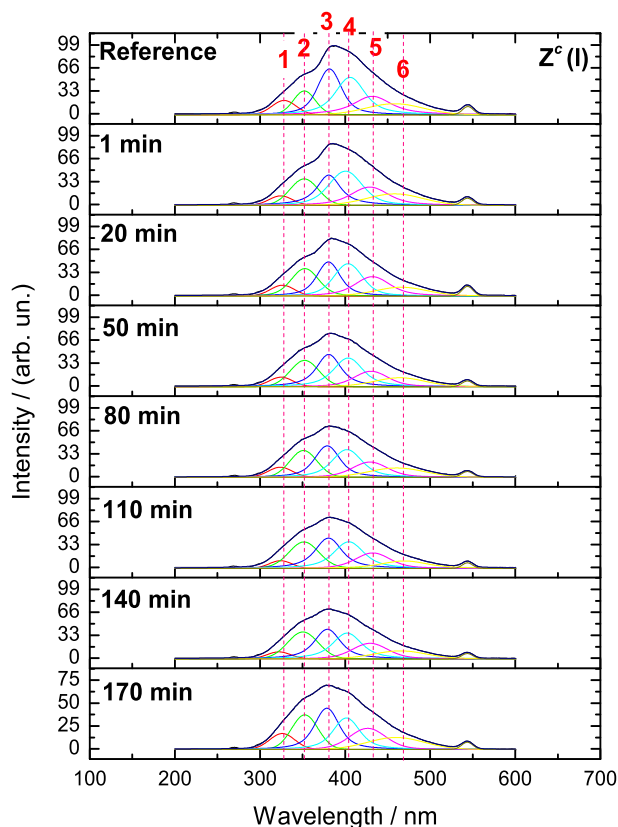
Fig. 2. PL spectra from Z^c(l) with respect to time evaluated at λ_{ex} = 275 nm. The first measurement was achieved as reference by only measuring the PL emission from Z^c(l) prepared as in section 2.2.1. After 1 minute 1 mL of water, in this case, was added to later measure spectra at every time showed in this figure. Each peak was identified with a red number at the top of figure, corresponding to description in this section.

a slightly increase in the emission is attained in both λ_{ex}. In this case, after GQD incorporation, recombination from V_O^x is preferred indicating the possibility that some of these defects are fairly near the ZnO surface.

(F) Peak at 454 nm. Intrinsic vacancies in Z^d(s) produce an emission in the blue visible region. A difference between Z^d(s) and Z^c(s) spectra is registered and is associated to vacancies created by the calcination process. The decrease in PL emissions in Z^c(s) and Z^cDl-3(s) is associated with these vacancies which might be acting as electron-traps inhibiting electronic transitions. Moreover, when H_2O_2 is added an increase in the emission intensity is not observed. Opposite to peak at 440 nm, when high concentration of H_2O_2 is added, the possibility to cover the intrinsic and new vacancies is very low, as the PL intensity is lower in Z^d:1(s) than Z^d(s). Therefore, we consider that these vacancies are deeper than those found at 440 nm. Thus, this is the reason that these vacancies, are more stable, leading to red-shift emission [35]. Therefore, these vacancies should be at the ZnO bulk preventing diffusion of oxygen or other gases.

(G) Peak at 478 nm. This peak remains after H_2O_2 addition to Z^dDl:1(s) and Z^d:1(s), relative to 415 nm peak (Fig. 1b). Therefore, neither oxygen nor hydrogen might affect these sites. Again, this peak is related to deep-level oxygen vacancies which are chemically stable to H_2O_2 and are related to green luminescent emissions [25].

3.2. Parallelism of emission source from solids to samples in liquid phase

In this section we measured the PL in aqueous phase to observe stability of nanocomposites. In general terms, in this work stability includes photostability which defines if samples are not chemically modified by photons and chemically stable, which here is the extend that nanocomposites might last before being affected by H_2O_2. The emission spectra taken at λ_{ex} = 275 nm, are shown in Fig. 2 for Z^c(l) in liquid phase. For each spectrum, six peaks were found to fit well the experimental data. Therefore, from the solids spectra in Fig. 1, it is possible to assign the emission peaks from samples in liquid phase and they might be related with the same chemical environment from the ZnO structure treated in section 3.1. Because H_2O_2 was not used for Z^c(l), it is important to note the irregularity of the PL emission for all peaks in all the measurements (Fig. 2). Long time exposure to water, provoked a mild chemical modification in Z^c(l) which affects the PL emission.

It is noteworthy to mention that the same PL peaks found in Z^c(l), were also displayed in the rest of samples and their plots are shown in Fig. S2. Results from Fig. S2 were condensed and are presented in Fig. 3, showing intensities for every peak found in these samples. If the first point (reference) is compared with the second point, which is after adding the H_2O_2 solution, a rapid effect is
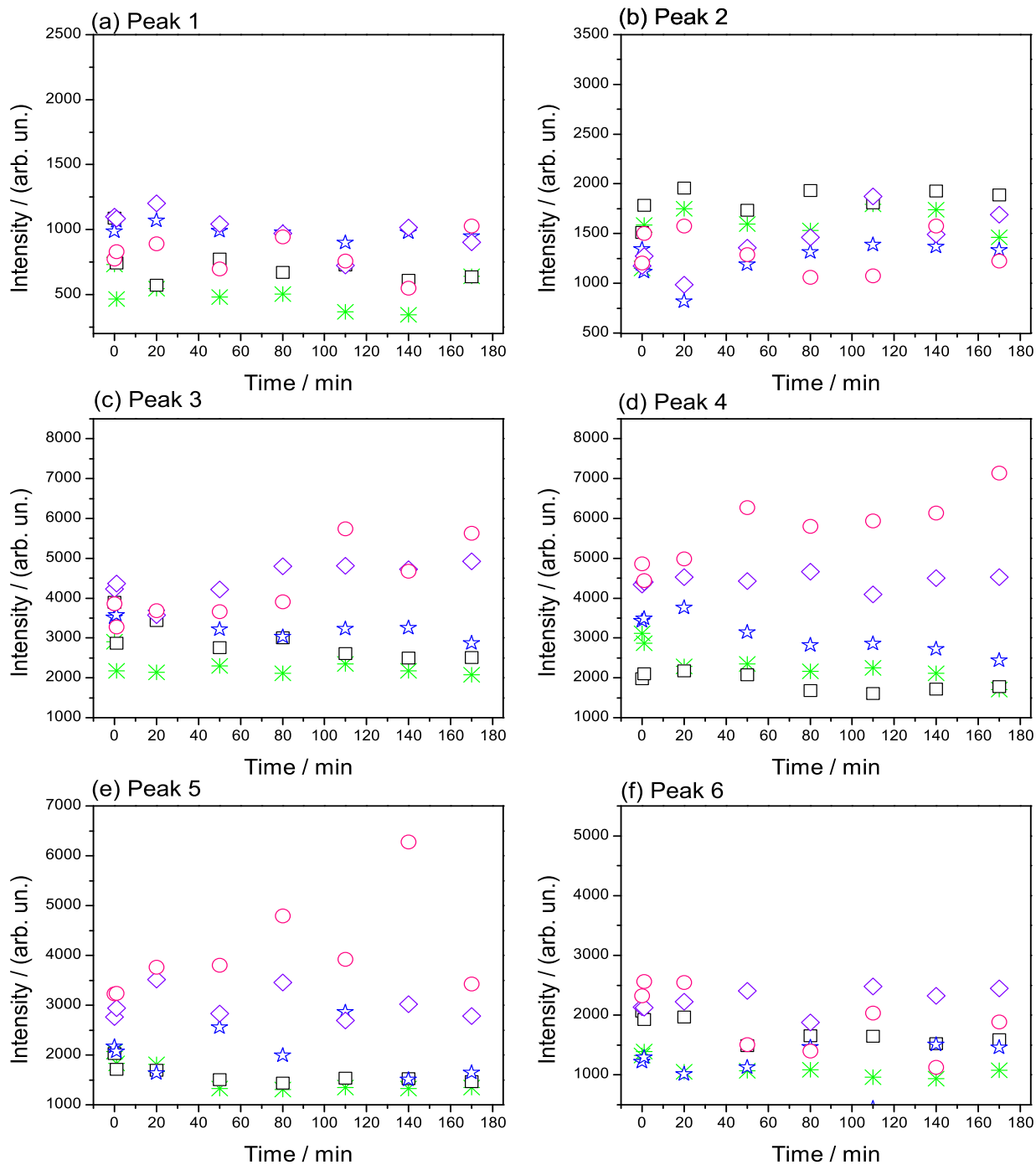
Fig. 3. Peaks intensities with respect to time from the spectra decomposition of samples Z^c(l) (∗), Z^c-3 (□), Z^cDl-3 (⋆), Z^cDm-3 (◇) and Z^cDh-3 (○). The far left points in each sample are the reference values (taken without H_2O_2) and the rest of measurements were done with a H_2O_2 solution (10^{-3} M); all evaluated at λ_{ex} 275 nm.

observed in each peak meaning that H_2O_2 acts immediately in almost all samples (where Z^cDm-3 seems to be an exception). Then, variations in intensities over time, must be related with chemical environment variations provoked by H_2O_2, principally in ZnO structure. Thus, these six peaks from Fig. 3 are described as follows:

Peak 1 Opposite to PL emission in solid phase (Fig. 1), samples in liquid phase for peak 1 (Fig. 3a), present emissions even at low H_2O_2 concentrations. The H_2O_2 improves the PL intensity in all samples, whilst GQD have a minor effect. In Z^cDh-3 the PL emission is mildly lower than Z^cDl-3 probably due to GQD are impeding the H_2O_2 to reach the ZnO structure. For these reasons,

the emission peak 1, is therefore ascribed principally to ZnO due to a possible formation of an ORE at these sites where the excitation is occurring. Notwithstanding, interestingly GQD might be inducing to slightly increase the amount of bound exciton emission in ZnO (Fig. 3a). In this sense, exciton binding energy might emerge due to the presence of water, H_2O_2 and GQD.

Peak 2 In Fig. 3b, the intensity of peak 2 remains mainly constant almost for all samples except for Z^cDh-3. The emission emerging from this peak has low intensity but according to description of the emission peaks from Fig. 1, this peak is related also with the exciton-free and binding energy arising from interstitial hydrogen. It is clear that H_2O_2 tends to increase the emission in Z^c-3, pointing the effect of this oxidant, due to hydrogen reaction with surfaces as presented in scheme 1 in Fig. S1. GQD in the nanocomposites have also a small effect as in peak 1. Note how Z^cDl-3 and Z^cDm-3 present a mildly higher PL emission intensity than Z^cDh-3. In this situation, the ZnO surface is obstructed by GQD when is in higher concentration as in Z^cDh-3.

Peak 3 This peak is related with the PL emission from oxygen vacancies, which are prone to be perturbed by the presence of GQD (Fig. 3c). It is noted that $Z^c(l)$, shows a steady behaviour during the experiment, however, Z^c-3 presents a slightly higher intensity. This evidence suggests that ZnO is being attacked by H_2O_2 at low concentrations. Although Z^c-3 presents higher PL emission than $Z^c(l)$, this decreases with respect to time. As the peak 3 from solids, $HOO^.$ radicals adsorbed onto V_O decrease exciton transitions; however, this process is slower in liquid phase due to desorption of these radicals is difficult and thus, the diminishing in PL emission is achieved gradually. As mentioned in section 3.1 (Fig. 1), GQD are prone to interact with these sites and this is confirmed as they initially increase the emission in all nanocomposites. Notwithstanding, the later performance depends on the GQD concentration. In Z^cDl-3 a minor decrease in emission intensity is observed. On the contrary, Z^cDm-3 and Z^cDh-3, display an increase in intensity. As it was explained for the peak 2, a weak interaction from GQD in Z^cDl-3 must be related with the decreasing of PL intensity, whilst in Z^cDm-3 and Z^cDh-3, interaction must be stronger, due to they possess higher GQD concentration and thus, greater amounts of carboxyls groups which might be interacting and preventing the H_2O_2 to reach ZnO surface (Fig. S3); moreover, amine groups (identified in XPS see section 3.4) must be interacting with H_2O_2. Therefore, the GQD action must be a function of its concentration and, when its concentration is higher, its positioning at the ZnO surface may be time consuming to be complete; in Fig. S4a, this is confirmed in an experiment with Z^cDh:0 where no H_2O_2 was used and a similar performance although with lower intensity was displayed. This means that when H_2O_2 participates, a different configuration in GQD-ZnO-H_2O_2 interaction occurs due to an increase in intensity instead of decreasing effect is presented.

Peak 4 This peak is associated to an ORE at the surface of the ZnO crystal structure (Fig. 3d). From UV-Vis spectra in Fig. 6, Dh presents two bands at 210 and 255 nm, associated to amine and $C=O$ groups, respectively. When GQD are in high concentration, these groups might reinforce the anchoring points at the surface of ZnO structure. Carboxyls groups are especially close to surface vacancies, serving as "*protection*" against H_2O_2, reducing the possibility of the ZnO surface oxidation by the attraction of amine groups to H_2O_2 (Fig. S3). Therefore, Z^cDh-3 contains a great amount of these functional groups bonding over the ZnO surface increasing the PL emission intensity. Notwithstanding, a gradual decrease in Z^cDl-3 is attributed to oxidation of ZnO surface by H_2O_2. With ZnO surface oxidation, the PL properties are lost due to a weak contact with GQD. In this sense, sample Z^cDm-3 might possess the right amount of GQD functional groups which anchor to the ZnO surface remaining the nanocomposite chemically stable during the experiment. This is the reason why this sample is the ideal to be used as H_2O_2 photoluminescent sensor and the peak 4 is related to the effects of H_2O_2 that might cause a perturbation in the PL properties.

Peak 5 The peak 5, related to oxygen vacancies, is perturbed by H_2O_2 specially with long times, and low or high GQD concentration (Fig. 3e). It is observed that once GQD seem to be close at these sites PL emission increases for Z^cDh-3 to decrease after 80 minutes. For Z^cDl-3 and Z^cDm-3, the behaviour is almost similar to Z^cDh-3 however more unsteady. This decreasing in PL intensity, is ascribed to H_2O_2 which principally interacts with GQD instead with ZnO and this is proved as Z^c-3 and $Z^c(l)$ have very similar performance.

Peak 6 Finally in peak 6, as well associated to oxygen vacancies at the bulk from ZnO, might be reached by radicals from H_2O_2 (Fig. 3f). Sample Z^c-3 has higher PL emission intensity compared with $Z^c(l)$. This arises from the incorporation of $HOO^.$ close to these sites. Increment of emission is only mildly dependent of GQD concentration. For Z^cDh-3 and Z^cDm-3, GQD must not be interfering with these sites, however in Z^cDl-3 they might be impeding the diffusion of these radicals. In this way, GQD from Z^cDl-3 might prefer these sites and this situation is not given for the other nanocomposites. In this respect, GQD which sizes are between 4 and 6 nm (Fig. S4b, Fig. S4c and Fig. S4d) are candidates to be interacting very close to these sites.

In general, it seems that in peaks 1 and 2 the effect of GQD is negligible. Moreover, as it was mentioned, water produces only a small effect on ZnO PL emission therefore differences between $Z^c(l)$ and Z^c-3 must be ascribed due to the $HOO^.$ and H^+ at the interstitials which enhances exciton formation. For peaks 5 and 6, it seems that longer times influence to gases or H^+ reach bulk vacancies faster. Whilst after calcination, vacancies created at the surface (or close to surface) of ZnO may interact with GQD. However, because these interactions are very weak GQD are attaching when PL emission increases and detaching when PL emission decreases. Because peaks 5 and 6 resembles emission peak at 454 nm for these solids samples, the similarities of $Z^c(s)$ and $Z^d(s)$, are that because vacancies at the bulk are presented in both samples they must show emission at the middle of visible spectrum; however close to the high energy of this spectrum, they show difference because $Z^d(s)$ possess less vacancies near the ZnO surface. This is because hydroxyls and in a lesser extension, carbonates, act as electron traps enhancing the PL emission.

3.3. Structural and morphological transformations of materials

During the synthesis of ZnO, the $Zn(OH)_2$ phase might be also formed due to the process humidity and high pH. This can be corroborated in a XRD pattern for Z^w in Fig. S5 where most of these peaks correspond to $Zn(OH)_2$ [36]. After low drying temperature,
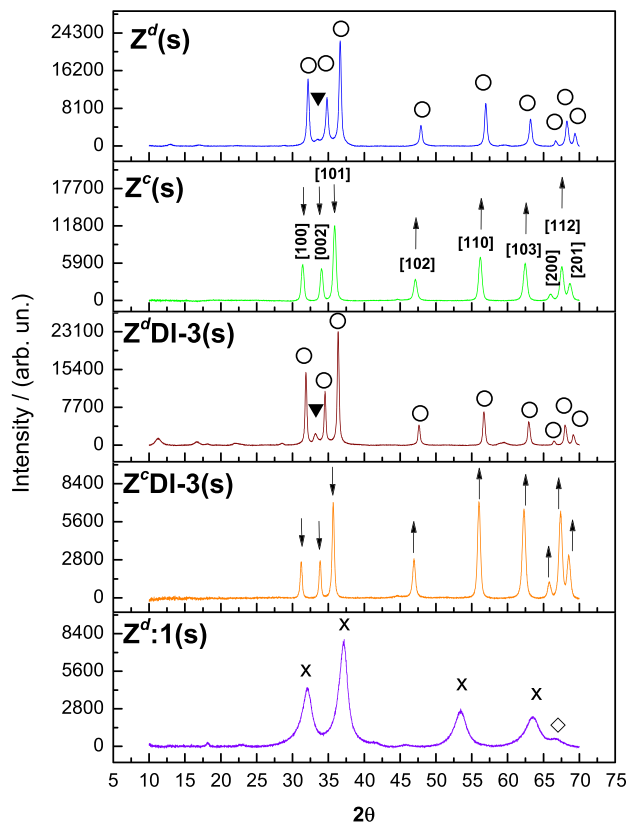
Fig. 4. XRD of Z^d(s), Z^c(s), nanocomposites Z^dDl-3(s) and Z^cDl-3(s) and Z^d:1(s); the identified phases in the first four samples are, ZnO phase (○) and *hydrozincite*(▼) and in Z^d:1(s) phases are ZnO_2 (×) and $Zn(OH)_2$ (◇).

spontaneous $Zn(OH)_2$ decomposition into ZnO occurred as is shown for Z^d(s) in XRD studies (Fig. 4); however, a portion of the initial solid was transformed into *hydrozincite* phase ($Zn_5(CO_3)_2(OH)_6$) which is marked with an inverted black triangle. Owing to the high temperature of calcination in Z^w (500 °C for 2 h), it was possible to remove more *hydrozincite* phase as this peak is not present in XRD pattern of Z^c(s) (Fig. 4). The sample Z^c(s), in fact, shows characteristic peaks from ZnO which correspond to *zincite* phase; this specific pattern is typical from ZnO nanoparticles (ZnNP) and all planes correspond to ZnNP peaks [37]; the ZnO attainment was corroborated in a differential scanning calorimetric (DSC) shown in Fig. S6a similar to one from literature [38]. The removal of carbonates and hydroxyls by calcination, is the most feasible process to provoke a lattice reconstruction and favour the growth in the direction of planes with upside arrows (Fig. 4 Z^c(s)). Besides of the loss of hydroxyls and carbonates, during this process, vacancies are also produced by the release of lattice oxygen from the Zn-O bond [39], rising the number of vacancies. With the generation of vacancies, a slight reduction of the crystal size was achieved in Z^c(s) (Table S1). This coincides with a theoretical study where it was found a strong relation among the diminishing of crystal size and the easiness to form oxygen vacancies because of the low energy required [40]. However, as is observed in SEM images, for Z^c(l) clusters of zinc oxide particles are produced whilst in Z^c-3 are not. Therefore, H_2O_2 cause clusters to split (Fig. 5) and with exposure to a 1 M H_2O_2 solution, ZnO_2 is produced, as is shown for Z^d:1(s) in Fig. 4 and in a DSC analysis (Fig. S6b) which describes the ZnO_2 decomposition to ZnO [27,41]. Moreover, incorporation of interstitial hydrogen and oxygen into ZnO lattice by H_2O_2, increases the ZnO crystal size (Table S1). This reaction is disclosed by the decreasing intensity of the three first planes in nanocomposites Z^dDl-3 and Z^cDl-3. Comparing XRD patterns of Z^dDl-3 and Z^cDl-3 is clear that the diminishing of crystal size resulted from the calcination whilst H_2O_2 reduces clusters. When GQD are added to calcined ZnO and exposed to H_2O_2, a slightly increase in ZnO crystal size occurred (Fig. 4 Z^cDl-3(s), Table S1). Due to GQD are placed at the zinc oxide surface, they help to maintain particles closer producing clusters although in a smaller size compared with Z^c(l) (Fig. 5). Therefore, all modification to the ZnO crystal is mostly attributed to calcination and H_2O_2. This is in good agreement with the PL results previously presented, where the emissions from interstitials hydrogen and oxygen are independent of GQD; in other words, GQD are mostly placed at the sites corresponding to the emission from peak 4 (see section 3.2). This was confirmed with the experiment from sample Z^cDh:0, measured without H_2O_2 (Fig. S4a); it is noticeable that this sample performs almost the same as Z^cDh-3, however with a lower intensity due to H_2O_2 absence, limits GQD to reach the ZnO promptly (Fig. S3). Therefore, the H_2O_2 provokes newly, the crystal growth in planes from $2\theta = 45°$ and thereafter, whilst the first three peaks again decrease in intensity. In this case, a slight possibility for carboxyls or amine groups from GQD to be placed at surface vacancies from ZnO might exist due to a further decrease in peak intensities at $2\theta = 31.4°$, $34.0°$ and $35.8°$ (Fig. 4 Z^cDl-3(s)). In addition, the occupation of ZnO interstitials by oxygen or hydrogen during the contact with H_2O_2 also induces to a diminishing in these peaks intensities. The
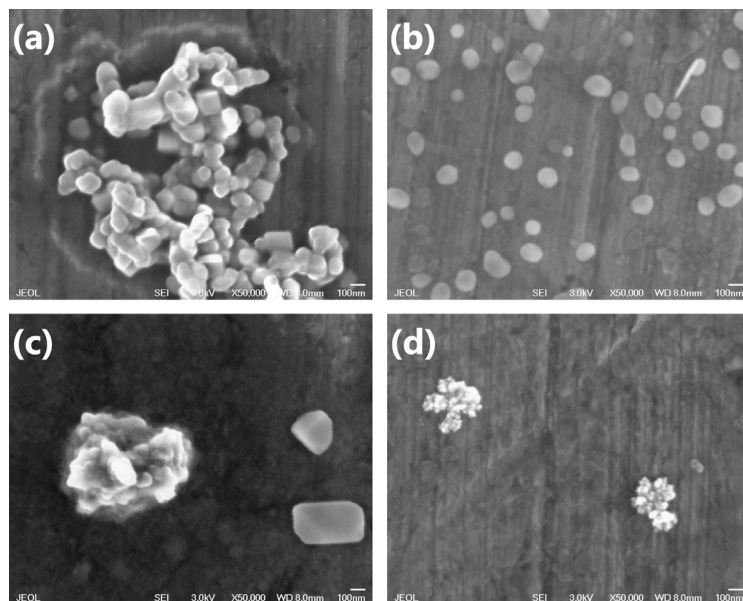
Fig. 5. SEM images from (a) Z^c(l) (b) Z^c-3 (c) Z^cDh:0 and (d) Z^cDm-3. Images in (a) are from ZnO crystals with different shapes, while H_2O_2 apparently tend to reduce the cluster size into smaller particles (b); for Z^cDh:0 in (c) H_2O_2 considerably reduced the clusters size which is shown in Z^cDh-3 (d). All samples were collected in aqueous phase and were placed in an aluminium substrate.

presence of a strong oxidant now might be oxidizing Zn creating an ORE in which small amounts of ZnO_2-like species are producing; this leads to new vacancies which finally results in a decrease of crystal size (Table S1); even, this coincides with the diminishing of particle size when samples are exposed to H_2O_2 as is shown in the SEM images (Fig. 5).

In Fig. 5, SEM images are shown to study the morphology of fresh and H_2O_2 processed samples. In Z^c(l) different shapes of ZnO particles are observed and due to the image scale, their sizes are around 100 nm (Fig. 5a). The growth process of ZnO consists in nucleation of ions and concentration of the zinc source where basic pH plays an important role. Inefficient stirring during the ZnO synthesis might be the causal to obtain particles of ZnO in prism and oval shapes [8] producing clusters of approximately 1 μm (Fig. S7a). From Fig. 5b smaller and well separated particles are noted for Z^c-3. This is evidence of the H_2O_2 action by modifying the morphology of the ZnO particles and reducing its size; similar variations in the ZnO morphology have been ascribed to structural defects which influence in the PL properties [42]. These defects are performed by the calcination and a posterior H_2O_2 exposure leading to a general enhancement of the PL properties. Although carbon was found in this sample, this enhancement was due to combination of vacancies, zinc, and oxygen (see EDS analysis for Z^c-3 from Fig. S7d). Contrary to Z^c(l), the appreciation from the Z^cDh:0 image (Fig. 5c) is that the clusters are smaller and enough separated. In this case GQD may prefer ovals-shaped particles and probably by a considerably attraction they maintain particles together and clusters totally separated; in Fig. S7f an EDS analysis of Z^cDh:0 registered a low amount of zinc (Table S2) which might imply zinc is covered by GQD. Notwithstanding these particles merge, in Z^cDm-3, the H_2O_2 break clusters reducing its size averaging 20 nm (Fig. 5d).

3.4. Chemical aspects from bulk and surface

In Fig. 6a, IR spectra show the bands corresponding to several chemical groups which are modified due to H_2O_2 or calcination. For instance, the first band corresponds to the O-H tension bonding which appears at 3347 cm^{-1}. In Fig. S11, the O-H band presented in Z^w, is notably higher in intensity compared with Z^d(s) and in fact this excess of OH, principally by water, avoids the spectrum sharpness. Only by drying the sample at 80 °C is possible to eliminate most of the superficially adsorbed O-H. This is ascribed to the chemical transformation from $Zn(OH)_2$ to ZnO as was corroborated in XRD and DSC studies of Z^w (Fig. 4 and Fig. S6). Once drying, O-H now are in a different arrangement and in this sense, the bands at 1550 and 1392 cm^{-1}, correspond to the $Zn_5(OH)_8Cl_2 \cdot H_2O$ complex in Z^d(s), which has been registered in other studies [43,44]. Now these bands are also exhibited in Z^dDl-3(s), although a higher intensity is attained in the nanocomposite than in Z^d(s). This is attributed to the HOO$^\cdot$, present in Z^dDl-3(s), thanks to H_2O_2. In fact, for Z^d:1(s) this band is even more intense confirming the action of these radicals (Fig. 6a). Moreover, in Z^d:1(s) the presence of O-H is manifested also at 3347 cm^{-1}; the amount of oxidant is too high in Z^d:1(s) that not only might incorporate more O-H at the surface and as complexes, but also generates the peroxide group (O-O) to appear at 1370 cm^{-1}. With this, it is possible an oxygen rich environment (ORE), which is related with the increase in emission when H_2O_2 is added during the PL experiments. Now, note that in Z^dDl-3(s), H_2O_2 is not enough to put these O-H groups at the surface in bands at 3347 and 1630 cm^{-1}, but interestingly the complexes corresponding to bands at 1550 and 1392 cm^{-1}, are even also more intense. Owing to carboxyls are present in non-calcined samples, with the incorporation of HOO$^\cdot$ radicals, carboxyls must be bonding to these radicals to form carbonates. In this sense, the *hydrozincite* is produced when H_2O_2 is added to the dried sample [27,45]. Winiarski et al. showed a similar IR spectrum
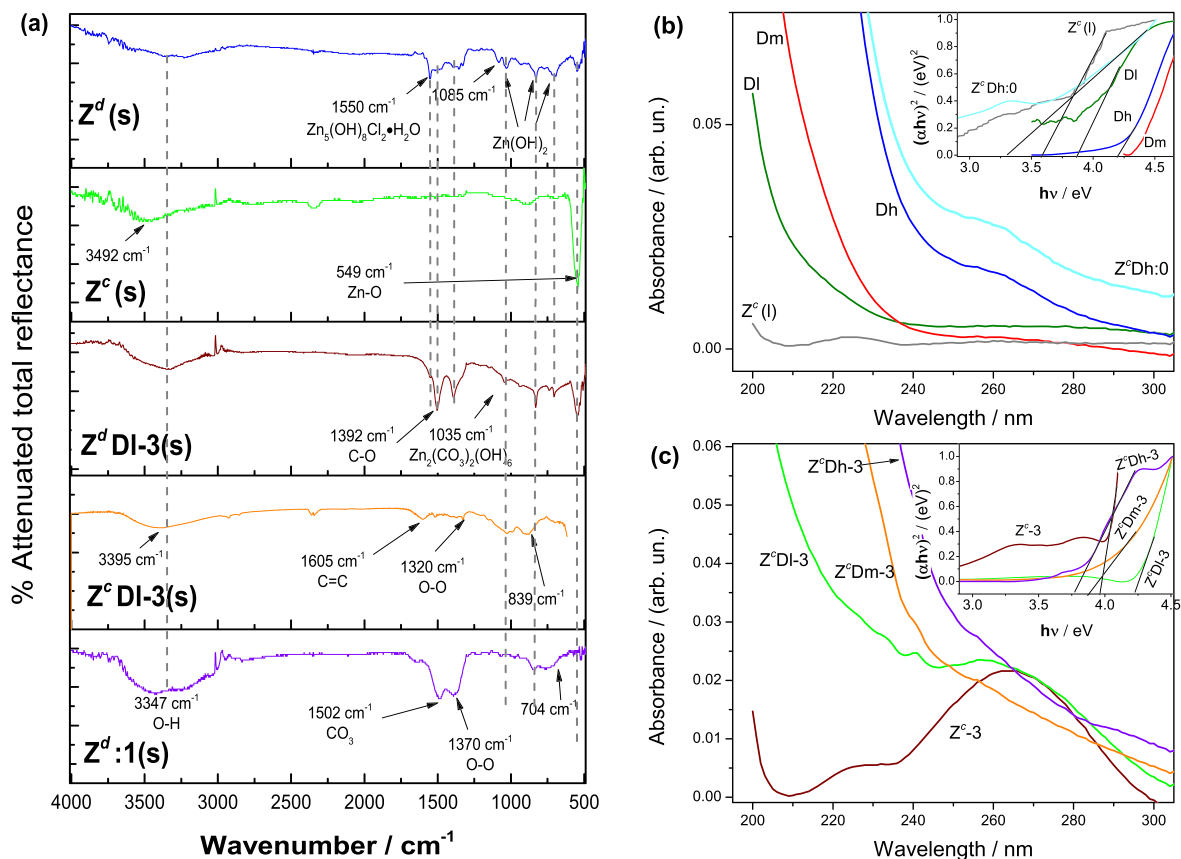
Fig. 6. (a) FTIR spectra where bands in general are associated to carboxyls or carbonates (from 1550 cm^{-1} to 1391 cm^{-1}), to hydroxyls (from 1093 to 739 cm^{-1}) and to ZnO (at 550 cm^{-1}). (b) UV-Vis spectra for low, medium and high GQD concentrations, Dl, Dm and Dh, respectively, Z^c(l), Z^{c}Dh:0 and (c) UV-Vis spectra for Z^c-3, Z^{c}Dl-3, Z^{c}Dm-3 and Z^{c}Dh-3; insets in (b) and (c) are the Tauc plot for these samples. Note: the UV-vis spectra were measured after the PL time experiments from section 3.2 were achieved.

corresponding to the _hydrozincite_ phase [43] and coincides with the evolution of the _hydrozincite_ peak for Z^{d}Dl-3(s) confirming the reaction of nanocomposites with H$_2$O$_2$ (Fig. 4). With calcination, all bands from carbonates and hydroxyls now are absent for Z^c(s) and, as carbonates were eliminated, it is believed that for Z^{c}Dl-3(s) the bands at 1035 and 839 cm^{-1} correspond to an ORE in which now zinc must be surrounded by peroxide radicals; in fact the O-O band is barely shown in Z^{c}Dl-3(s) at 1320 cm^{-1}. The vacancies due to carbonates elimination, might be now occupied by similar functional groups from GQD as the band at 1605 cm^{-1} is assigned to the C=C bond proving the interaction between ZnO and GQD [46,47]. This last bond is related with the red shift of the O-H bond from 3492 cm^{-1} for Z^c(s) to 3395 cm^{-1} in Z^{c}Dl-3(s). Note that both bands are at higher wavenumbers highlighting the calcination process, where only chemically bond O-H is on ZnO. The presence of C=C, produces the red shift of O-H for Z^{c}Dl-3(s) and we assign this to a strong ion-dipole attraction between carbon from GQD and oxygen from ZnO.

In Fig. 6b, UV-Vis spectrum for Dh shows an absorbance band at $\approx$ 260 nm which corresponds to $n-\pi^*$ transition originated by C=O groups [48]. In Dm and Dl this band has a very low absorbance value which is ascribed to the lower concentration of these samples. However, they present a band at $\approx$ 300 nm, assigned to an electronic transition occurring when nitrogen is present in GQD [48,49] proving the presence of the nitrogen groups in GQD. In Fig. S4c and Fig. S4d an AFM profile shows that GQD consists of structures around 5 nm which might be stacked in layers, building clusters between 20 and 100 nm (Fig. S12). That GQD are grouped in layers is related with the amine and carboxyls groups interaction. Inset of Fig. 6b shows band gap estimated by Tauc plots for GQD samples and their values are related precisely with an average particle size where the shorter particle size the higher band gap [50]. In this sense, Dm and Dh seem to have a smaller particle size than Dl, and this is ascribed to a probable higher repulsion maintaining particles well separated when GQD are in greater concentration in a solution. The sample Z^c(l) shows a very slight absorption at 265 nm which is assigned to Zn-O electronic transition [51]. For the nanocomposite Z^{c}Dh:0 we observe a stronger absorption compared to Dh at 265 nm and this is due to the interaction between these functional groups from GQD and Zn^{+2} [52]. Moreover, the greater ZnO particle size leads GQD to be more fixed when the nanocomposite is produced. Note that the band gap for Z^c(l) is 3.57 eV which is a slightly higher value than those reported in literature (3.2 eV) and this is attributed to fact that UV spectrum was measured after the PL time experiments. For Z^{c}Dh:0 the band gap decreases to about 3.29 eV which is also observed in literature when GQD are added to ZnO [13,19,21]. For Z^c-3 there is a notable absorption for the Zn-O (Fig. 6c) due to its exposure to H$_2$O$_2$. Note also that Z^{c}Dl-3 owing to the lowest GQD concentration, is similar to Z^c-3 and it developed a band at 262 nm which is assigned also to

Table 3

Atomic surface ratio with respect to oxygen peaks detected by XPS measurements.

Sample	O*	Zn2p$_{3/2}$/O1s		C1s/O1s		
		ZnO	Zn(OH)$_2$	-COOH	C-OH	C=C/C-C
Z^c(s)	O$_{lat}$	1.266	0.434	0.125	0.546	1.061
	O$_{sur}$	1.035	0.355	0.103	0.446	0.868
Z^{c}Dl-3(s)	O$_{lat}$	1.122	0.639	0.124	0.120	1.414
	O$_{sur}$	0.880	0.502	0.097	0.094	1.110
Z^{d}Dl-3(s)	O$_{lat}$	2.932	1.186	1.260	1.663	3.375
	O$_{sur}$	0.431	0.175	0.185	0.245	0.496

* Lattice oxygen peak (O$_{lat}$) and surface oxygen peak (O$_{sur}$)

Zn-O electronic transition. Samples Z^{c}Dm-3 and Z^{c}Dh-3 display a slight blue-shift respective Z^{c}Dl-3, although their bands are not as intense as in this last. When an ORE is occurring at the ZnO surface, the interaction between C=O and V$_O$ from ZnO, becomes weaker (Fig. S3); on the contrary for the other samples, C=O remain more strongly attached at the ZnO surface which diminish the absorbance from these groups. This is one of the reasons that PL properties in Z^{c}Dl-3 decrease with time in peaks 3 and 4 (Fig. 3). Similarly, the weaker intensity of this band, might be related with the formation of C-O-Zn bond which has been also proposed in other work [53]. Sample Z^c-3 possess a higher band gap value of 3.95 eV compared with Z^c(l) and as it was confirmed by XRD and SEM when particle diminishes, principally due to H$_2$O$_2$ incursion, band gap increases [22] (Inset of Fig. 6c). This is evidenced also for Z^{c}Dl-3 which is a similar sample and presents a band gap of 4.22 eV. The ZnO surface is more exposed in these samples and also, we confirmed this for Z^c:1(s) which was completely oxidized to ZnO$_2$ and its particle diminished to almost 6 nm as has been found in literature [54]. For Z^{c}Dm-3 and Z^{c}Dh-3 the band gaps diminished to 3.87 and 3.75 eV, respectively. Decrease in band gaps for these samples is attributed to ZnO surface protection granted by GQD.

Table 3 presents the atomic surface ratio (relative to oxygen) for samples Z^c(s), Z^{c}Dl-3(s) and Z^{d}Dl-3(s), obtained from decomposition of the peaks detected by XPS measurement presented in Fig. 7 and Fig. S13. XPS spectra from oxygen peak (O1s) emerges around a binding energy (BE) of 531 eV corresponding to lattice oxygen (O$_{lat}$) and a shoulder (at ≈ 532 eV) associated to surface oxygen (O$_{sur}$) contained in water or other chemical compounds [1,43] (Fig. 7a). In this figure, the red-shift in Z^{c}Dl-3(s), implies the oxygen distribution at the surface producing the new chemical environment in ZnO (Fig. 7b). Both peaks (O$_{lat}$ and O$_{sur}$) show variations related with a decrease in the Zn/O ratio for Z^{c}Dl-3(s) compared to Z^c(s) (Table 3). By this means, it is inferred that surface oxygen from ZnO, increases when H$_2$O$_2$ is added demonstrating the ORE condition.

The peak at a BE of 1021 eV (Fig. 7c) corresponds to zinc (Zn2p$_{3/2}$) and its decomposition is related to ZnO (≈ 1021.9 eV) and to zinc at BE of ≈ 1022 eV, where species as Zn(OH)$_2$ are preferentially formed [36,43]. Because the zinc-to-oxygen ratio in Z^{c}Dl-3(s) increases, the required oxygen to produce hydroxyl-zinc species is less than Z^c(s) and Z^{d}Dl-3(s). This is associated with the calcination of sample, which permits a chemical structure where might exist a greater diffusion of H$^+$ and HOO$^-$, and therefore the calcination is very important. This peak also might be associated with oxygen vacancies because we deduced that owing to the minimum need of oxygen to produce hydroxylate species, radical, oxygen and H$^+$, can be inserted at the surface vacancies of the ZnO structure. In this manner, we may note that the peak Zn2p$_{3/2}$ from Z^{c}Dl-3(s) shift slightly to a higher BE suggesting that zinc is readily oxidized, than zinc from Z^{d}Dl-3(s). This is achieved thanks to easiest contact among H$_2$O$_2$ and the zinc surface in Z^{c}Dl-3(s).

The carbon peak (C1s) is detected in Z^c(s), from calibration of XPS equipment, whilst in Z^{c}Dl-3(s) and Z^{d}Dl-3(s), GQD contribute to increase the amount (Table 3) at the surface; this indicates that with a simple mixing synthesis method it was possible to attach enough GQD to ZnO. This peak oscillates in the 284-286 eV range, where C=C from sp^2 hybridization of GQD, besides C-C bond, might be overlapping (Fig. 7d); moreover, this carbon can be rich in oxygen which are presented as shoulders in C1s as -COOH and C-OH [10,48,49,55]. Alike, it can be observed a lightly shift to higher BE in Z^c(s) and Z^{c}Dl-3(s), owing to this last, possess more carbonates species because the *hydrozincite* phase. Therefore, in Z^{d}Dl-3(s) the carbon amount is higher due to contamination as it was demonstrated by XRD and SEM analysis.

Finally, the nitrogen detected by XPS measurements confirms the presence of GQD at the ZnO surface (Fig. S14). Due to a low signal-to-noise ratio the amount of nitrogen at the ZnO surface was too difficult to estimate. However, the atomic amount detected by the XPS equipment was around 0.28% at the surface for both samples, demonstrating a properly functionalization by amine groups.

3.5. Analysis of H$_2$O$_2$ detection by photoluminescence

As it was determined in section 3.2, sample Z^{c}Dm-3 possess a steady performance in almost all peaks. For this reason, it was elected to prove the H$_2$O$_2$ effect in the PL, by varying its concentration. Fig. 8a, presents the effect of H$_2$O$_2$ in sample Z^{c}Dm:0 on the PL emission. In this experiment, a variation in H$_2$O$_2$ concentration was achieved and if Z^{c}Dm:0 and Z^c(l) are compared (Fig. 8a with Fig. 2) it can be noted that Z^{c}Dm:0 presents negligible variation in PL spectra. GQD might be protecting the ZnO structure and for this reason a similar shape in spectra is attained even though the H$_2$O$_2$ concentration is increasing (Fig. 8a). Spectra from Z^{c}Dm:0 can be decomposed in six peaks which correspond to the same peaks found in the description from section 3.2. The behaviour of these peaks is shown in Fig. 8b. In this figure peaks 1 and 6, which are respectively assigned to an ORE and to oxygen vacancies, display the lowest PL intensities. Notwithstanding, the PL emission from these sites, is not strongly perturbed by H$_2$O$_2$ concentration; also, as it was determined in peak at 478 nm (G) from section 3.1, the sites for peak 6 seem to be chemically stable to H$_2$O$_2$. As in
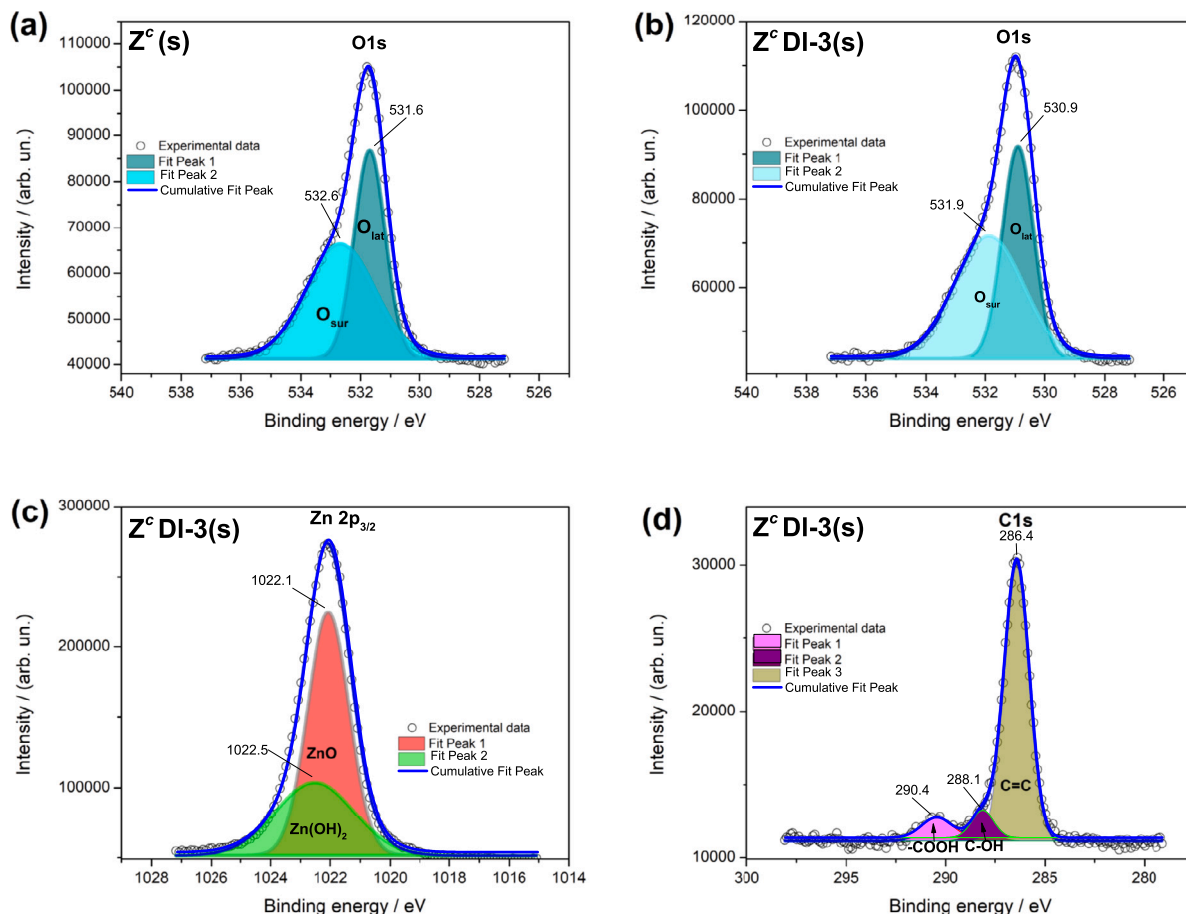
Fig. 7. XPS spectra from (a) Z^c(s), (b) Z^cDl-3(s) of the oxygen peak (O1s) and for the Z^cDl-3(s) of the (c) zinc peak (Zn $2p_{3/2}$) and the (d) carbon peak (C1s).

Fig. 3a and Fig. 3f, almost a steady performance is achieved, this means that these sites are not modified neither with time nor H_2O_2 concentration. Peak 2 is related with hydrogen at interstitials from ZnO structure. In this case, increasing the H_2O_2 concentration might also rise the proton generation; this situation would increase its diffusion into ZnO and should be a cause to increase the emission intensity. In fact, despite that this occurs, the growth of intensity is not as great as it was expected. This might be due to some of the H_2O_2 are already interacting with GQD placed at the sites of ZnO related to peak 4, which produce the quenching effect. Peak 5 is revealed when the calcination is done. Thus, vacancies generated by this process probably are near of the interstitials-hydrogen sites, but far enough of the ZnO surface; therefore, the vacancies are also chemically conserved as is observed that peak 5 in Fig. 8b behaves almost constant when H_2O_2 concentration increases. For peak 3 the H_2O_2 effect is more evident as when its concentration increases, emission intensity decreases. However, for concentrations of 0.001 M to 0.06 M in peak 3, the intensity is steady to decrease later again. This performance might be because of the ORE near the surface, where the oxygen provided mostly by H_2O_2, creates a new interaction with GQD by attracting amine groups instead of carboxyls. In this sense, a new chemical environment is produced where GQD are strongly bonded with ZnO surface and loss part of PL properties. In peak 4 sample Z^cDm-3 has a steady performance and for this reason, it was elected to prove the H_2O_2 effect in the PL, by varying its concentration. Immediately is noted the difference among the interaction of H_2O_2 with this solid when the oxidant concentration is varied and when time is passing. With time, emission remains steady, denoting that is chemically not modified; on the contrary, when concentration of H_2O_2 varied, a diminishing in PL emission is noted in Fig. 8c. The first point, which is the PL emission when only Z^cDm:0 and water is measured (raw) is far from the fitting line and from the next three points; notwithstanding, those following three points, along with the sixth measurement, fit well to a linear equation. The first and fifth point are not adjusted to the line probably due to a failure in the measurements. The last point, which was measured using a H_2O_2 concentration of 0.1 M, is well measured, however, might be the limit where a good quenching effect is achieved. In this sense, when H_2O_2 exceeds in concentration, a chemical modification in nanocomposite interferes with the analysis making it non-confident.

3.6. Interaction of ZnO and GQD by variations in band gap

Analysing the band gap from 6b and 6c insets, it is possible to conceive how the interaction among ZnO and GQD is taking place; this is represented in Fig. 9. Setting the conduction (CB) band of this solid with a value of - 4.20 eV [13], a value of the valence band
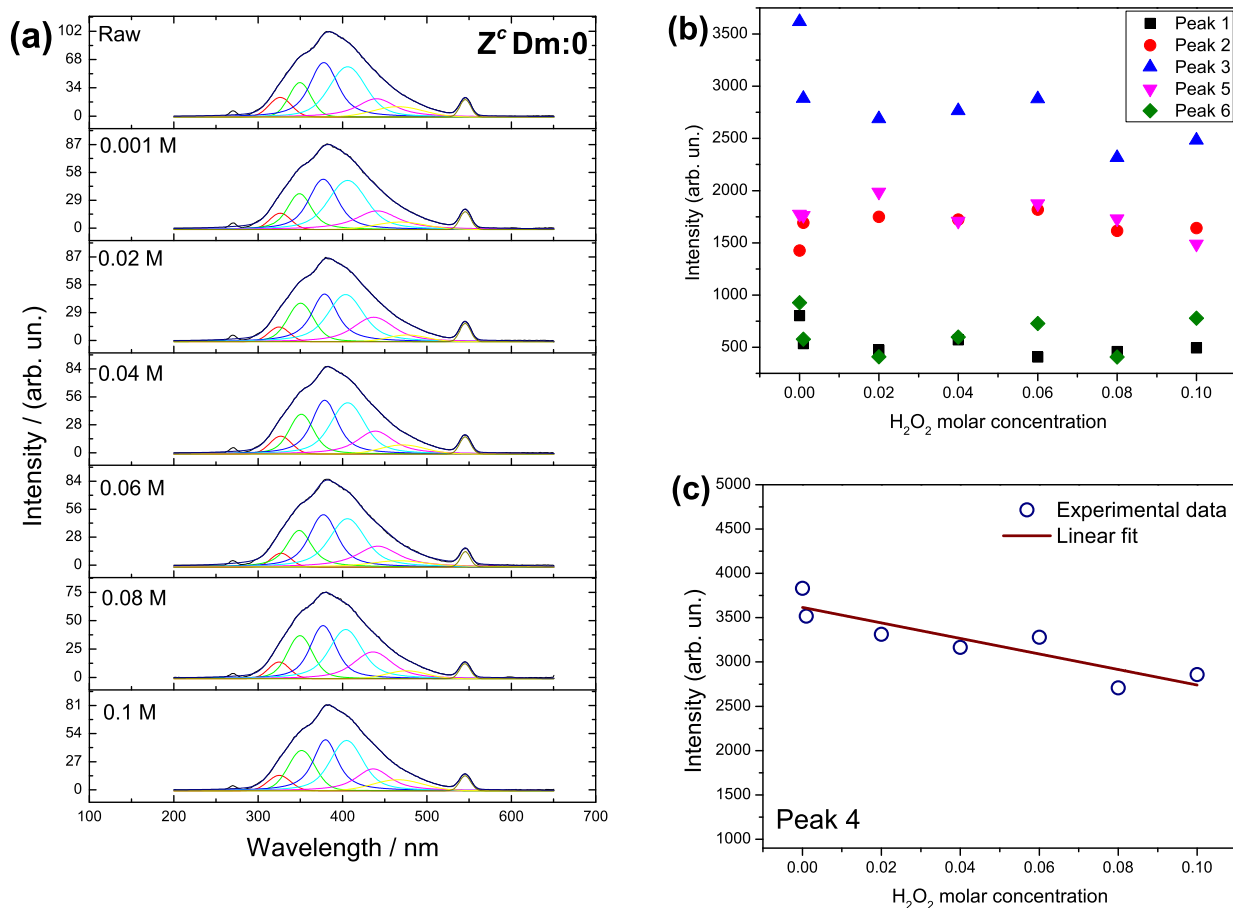
Fig. 8. (a) PL spectra from Z^{c}Dm:0 evaluated at λ_{ex} = 275 nm; the first measurement (raw) was achieved without H$_2$O$_2$ and in posterior measurements consisted in varying the H$_2$O$_2$ concentration; the six identified peaks, correspond to description in section 3.2 (b) intensities from peaks displayed in (a) and (c) peak 4 experimental intensities (○) and linear fit (wine line) which correspond to equation $I = -8762.2c + 3616.2$ with R^2 = 0.80, where I is the intensity of PL emission and c is the H$_2$O$_2$ concentration.

(VB) of - 7.77 eV it is found. From the CB of ZnO we found a VB value of - 8.15 eV for Z^c-3 which is ascribed to the generation of vacancies by H$_2$O$_2$ and to the diminishing of particle size. Also, by setting -5.35 eV the value for GQD [56] of the highest occupied molecular orbital (HOMO), the lowest unoccupied molecular orbital (LUMO) values are found to be - 1.49, - 1.07 and - 1.16 eV for Dl, Dm and Dh, respectively (Fig. 9). Because the band gap of ZnO might change during experiment, in Z^{c}Dl-3 the VB is -8.42 eV. This value is lower than Z^c-3 for which PL emission decreased. Moreover, charges produced in Dl are not energetically enough to be transferred to ZnO. In Z^{c}Dh-3 the ZnO band gap is the lowest (3.75 eV) in nanocomposites, and GQD might be contributing to increase the e-h recombination by transferring electrons to the CB of ZnO. From this perspective the highest LUMO value of Dm leads to conserve the e-h recombination for the nanocomposite Z^{c}Dm-3. Thus, in this process a compensation of electron loss by vacancies or non-radiative phenomena in ZnO is achieved with medium GQD concentration. Because of the electrostatic attraction between H$_2$O$_2$ (Fig. S3, scheme 3) PL intensity increases for Z^{c}Dh-3 displayed in Fig. 3d. Owing to sample Dl has the lower LUMO value in Z^{c}Dl-3, electrons of this sample might be only suffering an internal electronic transition. Besides that, vacancies in ZnO provoked by oxidation with H$_2$O$_2$ (in an ORE), inhibit the e-h recombination and thus PL emission is lost similarly as the Z^c-3 process showed in Fig. 3d. Although from Fig. S4a for Dh-3, GQD might be not disturbed by H$_2$O$_2$ an interaction among these compounds exists. This is because neither for Z^{c}Dm-3 nor Z^{c}Dh-3 a decreasing in PL emission is presented as in Z^c-3. In this manner, for Dm in Z^{c}Dm-3, e-h recombination is given in a similar form as in Z^{c}Dh-3; it is important to note that these recombinations are only favoured when the H$_2$O$_2$ concentration is maintained constant. In this respect GQD might also prevent the ZnO photoxidation which is associated with a strong bond between GQD and ZnO [53]. In literature, similar ZnO-GQD materials have been investigated and it has been found that charge is transferring from GQD to ZnO with a posterior e-h separation increasing the nanocomposite conductivity [12,18–20,22]. In our work is evident that this is not occurring due to e-h recombination has been enhanced in Z^{c}Dh-3 and it is conserved in Z^{c}Dm-3; we ascribe this to the small crystal size of ZnO. In these literature investigations the particle size ranges from 50 up to more than 1 µm. Besides the particle reduction, H$_2$O$_2$ exposure, provokes an anisotropic particle, which increases active sites where GQD are interacting [54]. These active sites are those related with peak 4 where GQD is interacting. Thus, we ascribed the enhancement of PL emission due to the small ZnO particle size.
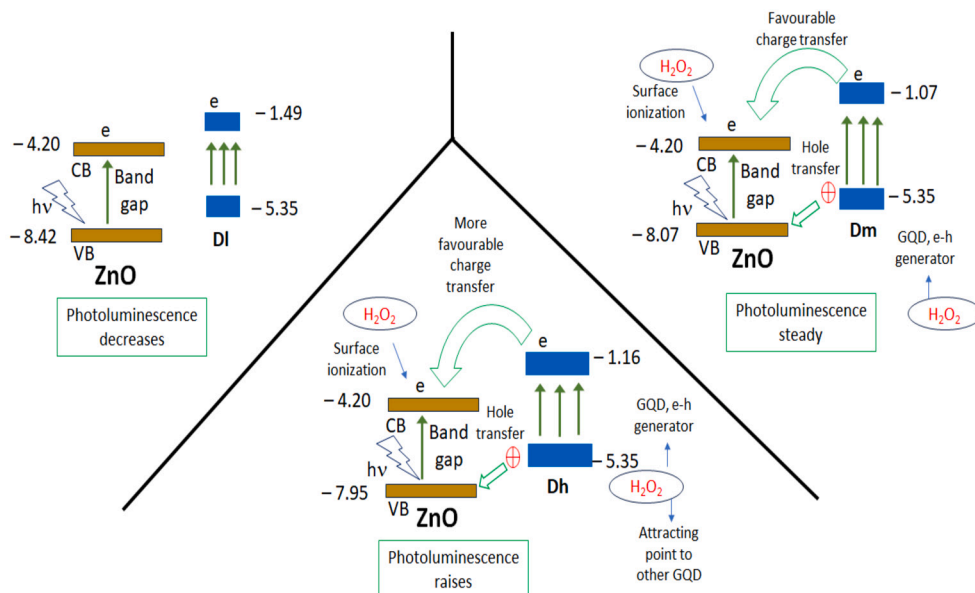
Fig. 9. Representation of the possible ZnO and GQD band gaps position. As the band gap from GQD is higher, PL intensity increases favouring e-h recombinations in ZnO. Values of VB, CB, HOMO and LUMO are in eV.

During nanocomposites synthesis GQD are bonded principally by carboxyl groups to ZnO surface, as it has been found in others works [52,53]. A DSC analysis was achieved in Z^cDl-3 sample showing an exothermic peak at 367 °C (Fig. S6c). Due to zinc carbonates and nitrates show a decomposition peak staring from 290 °C up to 350 °C we conclude that this peak must be from GQD carboxyl groups chemically bonded to Zn [53,57,58]. Moreover, when these groups are placed at the ZnO surface, it is not discarded that more GQD might be stacked producing layers. Therefore water, but principally H_2O_2 molecules, are attracted to GQD. In this investigation, HOO$^.$ radical from H_2O_2 is adsorbed on the ZnO surface decreasing the band gap in Z^cDh-3 and in Z^cDm-3, which is attributed to the fact that the ZnO was not attacked by H_2O_2 as in Z^c-3. However, since the emission intensity increases with time for Z^cDh-3 compared to ZDh:0, then H_2O_2 increases the number of recombination in Z^cDh-3 and in a lesser extent in Z^cDm-3. This is similar to other ZnO-GQD systems, where it has been found that an adsorbate (oxygen) at the ZnO surface, scarves free electrons from its surface [12,13,18,20]. However, in these works, later the adsorbate and electrons are released, when a hole produced by light excitation reach the ZnO surface. These e-h recombination in our work, must occur in the ZnO and not in GQD, otherwise an increase in the emission intensity would be seen in Dh-3 and this is not the case (Fig. S4a). Therefore, H_2O_2 must be interacting at the ZnO – GQD interface in such a way, that when the H_2O_2 arrives, peroxide ion produced and attracted at the ZnO surface while hydronium ion remains on GQD. The peroxide attracts or could even split another small particle from the GQD, which allows the addition of a new GQD particle that would participate in the reaction. Because this occurs mostly in Z^cDh-3 and less in Z^cDm-3 this last is the more indicated to have a steady performance for the H_2O_2 sensing. Is important to note that although in our results GQD transfer charge to ZnO, photocurrent is not produced due to these charges recombine again. Holes from GQD must be also being transferring to VB of ZnO contributing to the enhancement of e-h recombination. Because H_2O_2 might be decomposed into OH$^.$ and OH$^−$, they must be also aiding to recover electron and hole in GQD [46].

Once the H_2O_2 concentration increases, a quenching effect is produced (Fig. 8c) due to an excess of charges at the ZnO surface. This is an excess of peroxide, increasing electronic density. Thus, in the process of quenching for Z^cDm-3 a proper GQD amount is protecting ZnO but when H_2O_2 concentration rises, ZnO surface is surrounded by more H$^+$ and HOO$^.$. In addition, the alteration might be a layer depletion of the band energy from the ZnO surface, resulting when molecules as oxygen are adsorbed at the surface which provokes a facile movement from the holes to the surface enhancing the e-h nonradiative recombination [25].

4. Conclusions

In this study, an investigation of the interaction of ZnO and GQD was achieved by means of photoluminescence (PL) measurements. GQD interacted by carboxyls chemically bonded to Zn. This interaction was a function of GQD concentration and depended on the ZnO vacancies. Vacancies were created principally by calcination and slightly by the H_2O_2 exposure when produced an oxygen rich environment (ORE) at the ZnO surface. This ORE altered GQD environment depending on its concentration in nanocomposite. In low GQD, an ORE oxidized the ZnO surface weakening interactions of GQD-ZnO which decreased the PL emission. GQD in high concentration remained attached to ZnO surface and H_2O_2 only aided to more GQD particles reach ZnO increasing the PL emission. H_2O_2 diminished the ZnO-GQD particle size creating more vacancies rising interactions between ZnO and GQD. In this respect, GQD might prefer oval-shapes ZnO particles as was deduced by SEM. Only medium GQD concentration displayed a stable PL emission during 170 min. GQD might be placed chemically at ZnO surface vacancies, where exciton transitions occurred around 400 nm; here,

amine groups contained in GQD, passivated nonradiative traps. The growth of the GQD band gap, enhanced the charge transfer to ZnO increasing the PL emission intensity. Raising the H_2O_2 concentration conduced to an inhibition of the charge transfer produced by the depletion in layer of the band energy from the ZnO surface.

CRediT authorship contribution statement

Rolando Efraín Ramírez Garza: Writing – original draft, Methodology, Investigation, Formal analysis, Data curation, Conceptualization. **Sara Luisa Rodríguez de Luna:** Writing – review & editing, Methodology, Investigation, Conceptualization. **Idalia Gómez:** Supervision, Project administration, Investigation, Conceptualization.

Declaration of competing interest

The authors declare that they have no known competing financial interests or personal relationships that could have appeared to influence the work reported in this paper.

Data availability

Data will be fully available on request.

Declaration of generative AI and AI-assisted technologies in the writing process

Authors declare that no generative artificial intelligence was used in this manuscript.

Acknowledgements

Appendix A. Supplementary material

Supplementary material related to this article can be found online at https://doi.org/10.1016/j.heliyon.2024.e31144.

References

[1] N.M. Hosny, I. Gomaa, M.G. Elmahgary, M.A. Ibrahim, ZnO doped C: facile synthesis, characterization and photocatalytic degradation of dyes, Sci. Rep. 13 (1) (Aug. 2023), https://doi.org/10.1038/s41598-023-41106-4.

[2] I. Hussain, N.B. Singh, A. Singh, H. Singh, S.C. Singh, Green synthesis of nanoparticles and its potential application, Biotechnol. Lett. 38 (4) (2015) 545–560, https://doi.org/10.1007/s10529-015-2026-7.

[3] N. Fathima, N. Pradeep, J. Balakrishnan, Green synthesis of graphene quantum dots and the dual application of graphene quantum dots-decorated flexible MSM p-type ZnO device as UV photodetector and piezotronic generator, Bull. Mater. Sci. 44 (1) (Feb. 2021), https://doi.org/10.1007/s12034-020-02326-w.

[4] V. Gurylev, T.P. Perng, Defect engineering of ZnO: review on oxygen and zinc vacancies, J. Eur. Ceram. Soc. 41 (10) (2021) 4977–4996, https://doi.org/10.1016/j.jeurceramsoc.2021.03.031.

[5] F. Khan, N. Akhtar, N. Jalal, I. Hussain, R. Szmigielski, M.Q. Hayat, H.B. Ahmad, W.A. El-Said, M. Yang, H.A. Janjua, Carbon-dot wrapped zno nanoparticle-based photoelectrochemical sensor for selective monitoring of h2o2 released from cancer cells, Mikrochim. Acta 186 (2) (Jan. 2019), https://doi.org/10.1007/s00604-019-3227-x.

[6] Y.-J. Lin, C.-L. Tsai, Y.-M. Lu, C.-J. Liu, Optical and electrical properties of undoped ZnO films, J. Appl. Phys. 99 (9) (May 2006), https://doi.org/10.1063/1.2193649.

[7] Mursal, Irhamni, Bukhari, Z. Jalil, Structural and optical properties of zinc oxide (ZnO) based thin films deposited by sol-gel spin coating method, J. Phys. Conf. Ser. 1116 (2018) 032020, https://doi.org/10.1088/1742-6596/1116/3/032020.

[8] G.R. Li, T. Hu, G.L. Pan, T.Y. Yan, X.P. Gao, H.Y. Zhu, Morphology-function relationship of ZnO: polar planes, oxygen vacancies, and activity, J. Phys. Chem. C 112 (31) (2008) 11859–11864, https://doi.org/10.1021/jp8038626.

[9] J. Grabowska, A. Meaney, K.K. Nanda, J.-P. Mosnier, M.O. Henry, J.-R. Duclère, E. McGlynn, Surface excitonic emission and quenching effects in ZnO nanowire/nanowall systems: limiting effects on device potential, Phys. Rev. B 71 (11) (2005) 115439, https://doi.org/10.1103/physrevb.71.115439.

[10] L.-Y. Lin, S. Kavadiya, B.B. Karakocak, Y. Nie, R. Raliya, S.T. Wang, M.Y. Berezin, P. Biswas, ZnO_{1-x}/carbon dots composite hollow spheres: facile aerosol synthesis and superior CO_2 photoreduction under UV, visible and near-infrared irradiation, Appl. Catal. B, Environ. 230 (2018) 36–48, https://doi.org/10.1016/j.apcatb.2018.02.018.

[11] M.K. Barman, P. Mitra, R. Bera, S. Das, A. Pramanik, A. Parta, An efficient charge separation and photocurrent generation in the carbon dot–zinc oxide nanoparticle composite, Nanoscale 9 (20) (2017) 6791–6799, https://doi.org/10.1039/c7nr01663h.

[12] D. Liu, H.-J. Li, J. Gao, S. Zhao, Y. Zhu, P. Wang, D. Wang, A. Chen, X. Wang, J. Yang, High-performance ultraviolet photodetector based on graphene quantum dots decorated zno nanorods/gan film isotype heterojunctions, Nanoscale Res. Lett. 13 (1) (Aug. 2018), https://doi.org/10.1186/s11671-018-2672-5.

[13] K. Rahimi, A. Yazdani, M. Ahmadirad, Graphene quantum dots enhance UV photoresponsivity and surface-related sensing speed of zinc oxide nanorod thin films, Mater. Des. 140 (2018) 222–230, https://doi.org/10.1016/j.matdes.2017.12.010.

[14] J.J.L. Hmar, T. Majumder, S. Dhar, S.P. Mondal, Sulfur and nitrogen co-doped graphene quantum dot decorated zno nanorod/polymer hybrid flexible device for photosensing applications, Thin Solid Films 612 (2016) 274–283, https://doi.org/10.1016/j.tsf.2016.06.014.

[15] S. Wang, M. Zheng, D. Jiang, H. Yuan, H. Chen, Y. Fan, F. Li, W. Zhang, L. Ma, W. Shen, Graphene quantum dot-sensitized gap@zno nanocomposite for high-performance uv photodetectors, J. Phys. D, Appl. Phys. 55 (39) (2022) 395108, https://doi.org/10.1088/1361-6463/ac7fc8.

[16] A. Kathalingam, H.M. Salman Ajmal, D. Vikraman, S.-D. Kim, H.-C. Park, H.-S. Kim, Graphene quantum dots-wrapped vertically aligned zinc oxide nanorods arrays for photosensing application, J. Alloys Compd. 853 (2021) 157025, https://doi.org/10.1016/j.jallcom.2020.157025.

[17] M. Hoang Tran, T. Park, J. Hur, Solution-processed zno: graphene quantum dot/poly-tpd heterojunction for high-performance uv photodetectors, Appl. Surf. Sci. 539 (2021) 148222, https://doi.org/10.1016/j.apsusc.2020.148222.

[18] B. Yang, J. Chen, L. Cui, W. Liu, Enhanced photocurrent of a zno nanorod array sensitized with graphene quantum dots, RSC Adv. 5 (73) (2015) 59204–59207, https://doi.org/10.1039/c5ra07836a.

[19] S. Kumar, A. Dhiman, P. Sudhagar, V. Krishnan, ZnO-graphene quantum dots heterojunctions for natural sunlight-driven photocatalytic environmental remediation, Appl. Surf. Sci. 447 (2018) 802–815, https://doi.org/10.1016/j.apsusc.2018.04.045.

[20] E. Wongrat, T. Nuengnit, R. Panyathip, N. Chanlek, N. Hongsith, S. Choopun, Highly selective room temperature ammonia sensors based on ZnO nanostructures decorated with graphene quantum dots (GQDs), Sens. Actuators B, Chem. 326 (2021) 128983, https://doi.org/10.1016/j.snb.2020.128983.

[21] L. Roza, V. Fauzia, M. Rahman, I. Isnaeni, P. Putro, ZnO nanorods decorated with carbon nanodots and its metal doping as efficient photocatalyst for degradation of methyl blue solution, Opt. Mater. 109 (2020) 110360, https://doi.org/10.1016/j.optmat.2020.110360.

[22] M.T. Efa, T. Imae, Hybridization of carbon-dots with ZnO nanoparticles of different sizes, J. Taiwan Inst. Chem. Eng. 92 (2018) 112–117, https://doi.org/10.1016/j.jtice.2018.02.007.

[23] Z. Zhang, H. Liu, L. Zhai, J. Wu, L. Li, Construction of BiOCl-TNTs photoelectrochemical sensor for detection of hydrogen peroxide, Chem. Phys. Lett. 811 (2023) 140177, https://doi.org/10.1016/j.cplett.2022.140177.

[24] R.E.R. Garza, S.L.R. de Luna, G.H. Padrón, I.G. de la Fuente, A "turn-off" photoluminescent H_2O_2 detection based on a zinc oxide–graphene quantum dot (ZnO–GQD) nanocomposite and the role of amine in the development of GQD, RSC Adv. 13 (32) (2023) 21808–21819, https://doi.org/10.1039/d3ra02355a.

[25] Z.-M. Liao, H.-Z. Zhang, Y.-B. Zhou, J. Xu, J.-M. Zhang, D.-P. Yu, Surface effects on photoluminescence of single ZnO nanowires, Phys. Lett. A 372 (24) (2008) 4505–4509, https://doi.org/10.1016/j.physleta.2008.04.013.

[26] M.M.J. Eliel, P.D. Francisco, M.J. Duarte, H.P. Guillermo, P. Nicolaza, Structure and optical properties of ZnO and ZnO_2 nanoparticles, J. Nano Res. 56 (2019) 49–62, https://doi.org/10.4028/www.scientific.net/jnanor.56.49.

[27] V. Alvarado-Pérez, L.I. Cabrera-Lara, G. López-Téllez, D. Mendoza-Anaya, S. Hernández-López, M. Camacho-López, ZnO to ZnO_2 transformation assisted by H_2O_2 at ambient conditions, Mater. Chem. Phys. 233 (2019) 180–184, https://doi.org/10.1016/j.matchemphys.2019.05.066.

[28] Y. Shin, M. Kim, J. Oh, M. Han, S. Kim, K. Chung, Hydrogenation and annealing effects in *n*-type ZnO bulk samples, J. Korean Phys. Soc. 53 (9(5)) (2008) 2504–2507, https://doi.org/10.3938/jkps.53.2504.

[29] P.B. Balbuena, S.R. Calvo, E.J. Lamas, P.F. Salazar, J.M. Seminario, Adsorption and dissociation of H_2O_2 on Pt and Pt −alloy clusters and surfaces, J. Phys. Chem. B 110 (35) (2006) 17452–17459, https://doi.org/10.1021/jp063027z.

[30] L. Pavesi, F. Martelli, D. Martin, F.K. Reinhart, Photoluminescence enhancement in post-growth hydrogenated $Ga_{1-x}Al_xAs$ (0≤x≤0.32) and GaAs/GaAlAs multilayer structures, Appl. Phys. Lett. 54 (16) (1989) 1522–1524, https://doi.org/10.1063/1.101339.

[31] Z.-M. Liao, K.-J. Liu, J.-M. Zhang, J. Xu, D.-P. Yu, Effect of surface states on electron transport in individual ZnO nanowires, Phys. Lett. A 367 (3) (2007) 207–210, https://doi.org/10.1016/j.physleta.2007.03.006.

[32] P. Erhart, K. Albe, A. Klein, First-principles study of intrinsic point defects in ZnO: role of band structure, volume relaxation, and finite-size effects, Phys. Rev. B 73 (20) (2006) 205203, https://doi.org/10.1103/physrevb.73.205203.

[33] J. Wu, F. Long, B. Tang, X. Tang, Electronic structure and ferromagnetic properties of Zn vacancies in ZnO screw dislocations: first-principles calculations, AIP Adv. 8 (6) (Jun. 2018), https://doi.org/10.1063/1.5034501.

[34] J. Ye, S. Gu, F. Qin, S. Zhu, S. Liu, X. Zhou, W. Liu, L. Hu, R. Zhang, Y. Shi, Y. Zheng, Correlation between green luminescence and morphology evolution of ZnO films, Appl. Phys. A 81 (4) (2005) 759–762, https://doi.org/10.1007/s00339-004-2996-0.

[35] J. Wang, Z. Wang, B. Huang, Y. Ma, Y. Liu, X. Qin, X. Zhang, Y. Dai, Oxygen vacancy induced band-gap narrowing and enhanced visible light photocatalytic activity of ZnO, ACS Appl. Mater. Interfaces 4 (8) (2012) 4024–4030, https://doi.org/10.1021/am300835p.

[36] M. Wang, L. Jiang, E.J. Kim, S.H. Hahn, Electronic structure and optical properties of $Zn(OH)_2$: LDA+U calculations and intense yellow luminescence, RSC Adv. 5 (106) (2015) 87496–87503, https://doi.org/10.1039/c5ra17024a.

[37] W. Muhammad, N. Ullah, M. Haroon, B.H. Abbasi, Optical, morphological and biological analysis of zinc oxide nanoparticles (ZnO NPs) using Papaver somniferum L, RSC Adv. 9 (51) (2019) 29541–29548, https://doi.org/10.1039/c9ra04424h.

[38] A. Gordeeva, Y.-J. Hsu, I.Z. Jenei, P.H.B. Brant Carvalho, S.I. Simak, O. Andersson, U. Häussermann, Layered zinc hydroxide dihydrate, $Zn_5(OH)_{10}·2H_2O$, from hydrothermal conversion of ϵ-$Zn(OH)_2$ at gigapascal pressures and its transformation to nanocrystalline ZnO, ACS Omega 5 (28) (2020) 17617–17627, https://doi.org/10.1021/acsomega.0c02075.

[39] X. Zhang, K. Hui, F. Bin, K. Hui, L. Li, Y. Cho, R.S. Mane, W. Zhou, Effect of thermal annealing on the structural, electrical and optical properties of Al–Ni co-doped ZnO thin films prepared using a sol-gel method, Surf. Coat. Technol. 261 (2015) 149–155, https://doi.org/10.1016/j.surfcoat.2014.11.043.

[40] J. Liu, F. Gao, L. Wu, H. Zhang, W. Hong, G. Jin, Z. Zhai, C. Fu, Size effect on oxygen vacancy formation and gaseous adsorption in ZnO nanocrystallites for gas sensors: a first principle calculation study, Appl. Phys. A 126 (6) (2020) 1–9, https://doi.org/10.1007/s00339-020-03643-x.

[41] S. Ali, R. Morsy, N. El-Zawawy, M. Fareed, M. Bedaiwy, Synthesized zinc peroxide nanoparticles (ZnO_2; -NPs): a novel antimicrobial, anti-elastase, anti-keratinase, and anti-inflammatory approach toward polymicrobial burn wounds, Int. J. Nanomed. 12 (2017) 6059–6073, https://doi.org/10.2147/ijn.s141201.

[42] T. Andelman, Y. Gong, M. Polking, M. Yin, I. Kuskovsky, G. Neumark, S. O'Brien, Morphological control and photoluminescence of zinc oxide nanocrystals, J. Phys. Chem. B 109 (30) (2005) 14314–14318, https://doi.org/10.1021/jp050540o.

[43] J. Winiarski, W. Tylus, K. Winiarska, I. Szczygieł, B. Szczygieł, XPS and FT-IR characterization of selected synthetic corrosion products of zinc expected in neutral environment containing chloride ions, J. Spectrosc. 2018 (2018) 1–14, https://doi.org/10.1155/2018/2079278.

[44] O.K. Srivastava, E.A. Secco, Studies on metal hydroxy compounds. II. Infrared spectra of zinc derivatives ϵ-$Zn(OH)_2$, β-ZnOHCl, ZnOHF, $Zn_5(OH)_8Cl_2$, and $Zn_5(OH)_8Cl_2·H_2O$, Can. J. Chem. 45 (6) (1967) 585–588, https://doi.org/10.1139/v67-097.

[45] B.L. Rivas, G.V. Seguel, C. Ancatripai, Polymer-metal complexes: synthesis, characterization, and properties of poly(maleic acid) metal complexes with Cu(II), Co(II), Ni(II), and Zn(II), Polym. Bull. 44 (5–6) (2000) 445–452, https://doi.org/10.1007/s002890070064.

[46] S. Phophayu, P. Pimpang, S. Wongrerkdee, S. Sujinnapram, S. Wongrerkdee, Modified graphene quantum dots-zinc oxide nanocomposites for photocatalytic degradation of organic dyes and commercial herbicide, J. Reinf. Plast. Compos. 39 (3–4) (2019) 81–94, https://doi.org/10.1177/0731684419891245.

[47] D.L. Pavia, Introduction to Spectroscopy, Harcourt College Publishers, 2001.

[48] E. Hwang, H.M. Hwang, Y. Shin, Y. Yoon, H. Lee, J. Yang, S. Bak, H. Lee, Chemically modulated graphene quantum dot for tuning the photoluminescence as novel sensory probe, Sci. Rep. 6 (1) (2016) 1–10, https://doi.org/10.1038/srep39448.

[49] S.R.M. Santiago, T.N. Lin, C.H. Chang, Y.A. Wong, C.A.J. Lin, C.T. Yuan, J.L. Shen, Synthesis of n-doped graphene quantum dots by pulsed laser ablation with diethylenetriamine (deta) and their photoluminescence, Phys. Chem. Chem. Phys. 19 (33) (2017) 22395–22400, https://doi.org/10.1039/c7cp03993j.

[50] H. Kang, D.Y. Kim, J. Cho, Top-down fabrication of luminescent graphene quantum dots using self-assembled Au nanoparticles, ACS Omega 8 (6) (2023) 5885–5892, https://doi.org/10.1021/acsomega.2c07683.

[51] S. Talam, S.R. Karumuri, N. Gunnam, Synthesis, characterization, and spectroscopic properties of ZnO nanoparticles, ISRN Nanotechnol. 2012 (2012) 1–6, https://doi.org/10.5402/2012/372505.

[52] S. Vempati, A. Celebioglu, T. Uyar, Defect related emission versus intersystem crossing: blue emitting ZnO/graphene oxide quantum dots, Nanoscale 7 (38) (2015) 16110–16118, https://doi.org/10.1039/c5nr04461h.

[53] A. Tayyebi, M. outokesh, M. Tayebi, A. Shafikhani, S.S. Şengör, ZnO quantum dots-graphene composites: formation mechanism and enhanced photocatalytic activity for degradation of methyl orange dye, J. Alloys Compd. 663 (2016) 738–749, https://doi.org/10.1016/j.jallcom.2015.12.169.

[54] L.P. V., V. Rajagopalan, A new synergetic nanocomposite for dye degradation in dark and light, Sci. Rep. 6 (1) (Dec. 2016), https://doi.org/10.1038/srep38606.

[55] D. Oh, S. Shin, C. Lim, D. Hwang, Dopamine-mediated sclerotization of regenerated chitin in ionic liquid, Materials 6 (9) (2013) 3826–3839, https://doi.org/10.3390/ma6093826.

[56] Y.D. Shang, X.H. Chen, W.H. Ma, S.Y. Li, Y.C. Wang, F.W. Xiang, Preparation and optical properties research on graphene quantum dots, Key Eng. Mater. 727 (2017) 303–308, https://doi.org/10.4028/www.scientific.net/kem.727.303.

[57] M. Pudukudy, Z. Yaakob, R. Rajendran, T. Kandaramath, Photodegradation of methylene blue over novel 3D ZnO microflowers with hexagonal pyramid-like petals, React. Kinet. Mech. Catal. 112 (2014) 527–542, https://doi.org/10.1007/s11144-014-0703-5.

[58] K.E. Levine, B.J. Collins, M.D. Stout, M. Wyde, S.E. Afton, A.S. Essader, T.J. Ennis, K.E. Amato, A.C. McWilliams, B.L. Fletcher, R.A. Fernando, J.M. Harrington, N. Catlin, V.G. Robinson, S. Waidyanatha, Characterization of Zinc Carbonate Basic as a Source of Zinc in a Rodent Study Investigating the Effects of Dietary Deficiency or Excess, Anal. Lett. 50 (2017) 2447–2464, https://doi.org/10.1080/00032719.2017.1293073.